CIRP Journal of Manufacturing Science and Technology 42 (2023) 72–80

Contents lists available at ScienceDirect

CIRP Journal of Manufacturing Science and Technology

journal homepage: www.elsevier.com/locate/cirpj

A novel approach for simulating a sawing process with reduced simulation time

Hans-Christian Möhring [a], Christian Menze [a,*], Konstantin Drewle [a], Dennis Fackelmann [a], Jan Stegmann [b], Stephan Kabelac [b]

[a] Institute for Machine Tools, University of Stuttgart, Holzgartenstrasse 17, 70174 Stuttgart, Germany
[b] Institute of Thermodynamics, Leibniz University Hannover, An der Universität 1, 30823 Garbsen, Germany

ARTICLE INFO

Available online 2 March 2023

Keywords:
Cutting simulation
Sawing
Simulation time reduction

ABSTRACT

The numerical simulation of machining processes enables the analysis of thermo-mechanical effects and can be used to predict process-specific quantities such as cutting force and chip shape. This involves, however, a great amount of computational effort and time depending on the model design. Basically, a simulation can be carried out two- or three-dimensionally. Due to the lower computational effort, 2D simulations were often used in the past to analyse the machining properties. In orthogonal cutting, this leads to a good approximation to the real processes if a suitable ratio between cutting width and depth of cut is applied. Nevertheless, most industrially relevant machining processes cannot be completely simulated with a 2D simulation. For these purposes, 3D simulations must be created. This requires a much greater computational effort, which increases the simulation time. This paper shows an approach to determine the cutting force and the information about the chip shape during sawing (bound orthogonal cutting) with a shortened calculation time. This was achieved by dividing the entire cut into 2D and 3D areas. The ratio between the cutting width and the depth of cut defines the criterion for the division. When it was greater than 10, the cutting process between the corner radii was assumed to be a plane two-dimensional strain state. The results showed a good agreement of the cutting force calculated from the 2D–3D simulation approach with experimental investigations and a 3D simulation. The computing time could be reduced by more than 50%.

Introduction

Machining is one of the most common manufacturing processes for producing various components. The circular sawing process here is an important intermediate step in the manufacture of semi-finished products. Regarding the basic procedure of the sawing process, simulation tools such as the FEM simulation can be used to understand the sawing process more precisely and to predict thermo-mechanical properties such as forces and temperatures as well as the chip morphology and the chip compression ratio. In [1], a study was presented on the FE simulation of the circular sawing process for aluminium with the LS-Dyna software. The circular sawing process was directly implemented once, and the influence of the cutting speed on the cutting forces was investigated. However, the simulation was carried out without a temperature calculation. Subsequently, the authors abstracted the model of the circular sawing process as an orthogonal cut and identified the cutting edge as a temperature maximum, taking the temperature calculation into account. In [2], a sawing process of aluminium was simulated using SFTC DEFORM 3D. The focus was on examining the influence of the feed rate parameters on the resulting cutting forces, stresses and the temperature distribution in the workpiece. By means of the Coupled Eulerian-Lagrangian model (CEL), a circular sawing process with internal coolant supply was simulated [3]. This approach allowed the definition of several materials with different properties in the same Eulerian space. In this way, the fluid-structure interaction between chip and coolant could be modelled.

Advances in computing power have increased the application of numerical machining simulations. Arrazola et al. [4] showed the significant progress in modelling machining processes since 1998 [5]. Cutting simulations can be carried out with mesh-based, continuum-mechanical Lagrangian approaches by an implicit [6] or explicit [7] simulation. To achieve chip removal, the Lagrangian models delete elements in the wider area of the tool radius. Element deletion can be invoked through the usage of certain material properties such as the damage initiation criterion and the damage

* Corresponding author.
E-mail address: Christian.menze@ifw.uni-stuttgart.de (C. Menze).

https://doi.org/10.1016/j.cirpj.2022.12.019

evolution. When the end of the damage evolution process has been reached, the element is deleted. To achieve premature deletion of the elements outside the tool radius, an intermediate layer was introduced with lower material values than in the rest of the workpiece regarding the damage regime [8]. Moreover, sophisticated remeshing routines can be used to consider the chip removal as a flow of material around the cutting edge [9]. Some commercial software packages offer this function (e.g. SFTC DEFORM, AdvantEdge). Arbitrary Lagrangian-Eulerian elements (ALE) combine the advantages of Eulerian and Lagrangian elements [10]. This formulation takes advantage of both views in that the motion of the material is generally independent from the mesh on top of it, but the mesh can also be moved and deformed. A very recent method of modelling machining processes is the CEL [11]. The special feature of the model lies in the fact that the workpiece is discretized in an Eulerian space, whereas the tool is modelled as a Lagrangian body. Originally reserved for modelling fluids, Eulerian spaces can handle great deformations of the underlying material [12]. The Eulerian mesh is stationary here, while the underlying material is moving through the mesh. By the usage of Eulerian elements, the otherwise occurring mesh distortions can be circumvented. Within the model, the tool is still represented as a Lagrangian body, hence the denotation.

However, Arrazola et al. [4] summarised that there is considerable need for the implementation of industry-compatible simulation models. Especially the transformation from 2D to 3D simulations should be an intensified research goal for the future. Much of the simulation research so far focuses on 2D orthogonal cutting. Although 2D FEM simulations have a great capacity for understanding the fundamental process mechanics in cutting [13–15], most industrially relevant machining processes (turning, milling, drilling, sawing) are three-dimensional. This paper presents a novel approach for reducing the simulation time by using a combined 2D and 3D simulation, based on the example of sawing. This was carried out by dividing the entire simulation area into inherent 2D and 3D sections.

Modelling approach

There are numerous different sawing processes, e.g. with set teeth or complex chip splitter grooves. To put it simply, the sawing process can be regarded as a bound orthogonal cutting process with engagement of the corner radius and the side cutting edges. Therefore, circular sawing has to be considered as a three-dimensional process. Thus, a plane 2D simulation cannot model the entire sawing process due to the impact of the corner radius and the side cutting edges. In a preliminary study, the stress and strain state in a bound orthogonal cut was investigated. For this purpose, a tool with a width of 4 mm and a corner radius of 0.4 mm was simulated in a bound orthogonal cut of AISI 1045 at a cutting speed of 100 m/min and a depth of cut of h = 0.15 mm. In the bound orthogonal cutting process with a corner radius (halved at the symmetry plane), the stress state in the primary shear zone was analysed in different planes, resulting in a stress profile that was largely constant along the width of cut (Fig. 1). Thus, the tooth engagement in the sawing process could be implemented in the area of the plane strain state (areas a - d in Fig. 1) with a 2D simulation and in the area of the cutting corner (area e in Fig. 1) with a 3D simulation.

To further investigate the physical properties in the deformation state of the bound orthogonal cut, the von Mises stress, the strain (in x-direction) and the temperature along an element path were taken into consideration. Fig. 2 shows the cut (without a tool) from the top (x-y-plane) and the rear (x-z-plane) as shown in Fig. 1. An element path was traced in x-direction through the chip near the secondary shear zone. Fig. 2 shows that the stresses and temperatures were almost constant from the symmetry plane (x = 0) to the position of x = 1 mm. The strain in x-direction was almost $\varepsilon = 0$. From x = 1 mm on, the temperature decreased slightly and the strain became negative up to the position of x = 1.6 mm (transition to the corner radius) with a minimum of $\varepsilon = -0.01$. The curve of these integral quantities showed that the range of a constant state between the corner radii can be assumed with good approximation.

A 2D simulation of orthogonal cutting is based on the assumption of a plane strain state inside (between the ends) of the cutting width and a plane stress state at the ends. When the width of a cut is large compared with its depth, side spread is concentrated at the edges and flow generally takes place in planes perpendicular to the work surface and parallel to the direction of cutting [16]. The ratio between the cutting width b and the depth of cut h generally determines whether such a stress-strain state is given.

$$w = \frac{b}{h} \tag{1}$$

In the past, different authors have proposed guideline values for the width-to-depth-of-cut ratio w. Shaw [17] claimed that machining can only be considered as being orthogonal when the width of the workpiece is at least five times greater than the depth of cut ($w \geq 5$). Oxley [18] recommended it to be ten times greater than the depth of cut ($w \geq 10$). Using FEA, Pednekar et al. [19] later increased the critical ratio w to 20.

In order to obtain cutting force information for sawing processes at a reduced simulation time, an approach was carried out for dividing the entire sawing process into a 2D and a 3D simulation as shown in the following. The idea was to simulate the bound orthogonal cutting process with two inherent simulations. For this purpose, the entire tool was divided into different areas (Fig. 3). The corner radius (right and left) was defined as a 3D area. In the area in between, a constant plane strain state was assumed. The area with constant plane strain distribution was represented with a 2D orthogonal cut. The areas at the cutting corners had to be represented with a 3D simulation due to the 3D stress/strain state. Finally, the results of the individual simulations were merged, and process information such as forces could be calculated as superposition of the single simulation results. The main question was whether the error in terms of process force values was acceptable compared to 3D simulations and real cutting results. In order to ensure that such a division was made on the basis of a physically correct assumption, a rule was needed to determine when such a division was reasonable.

The tool could be divided into three areas. The secondary cutting edges and the corner radius represented the areas in which a 3D behaviour existed (Fig. 3). The area in between (y) was defined as the area in which a plane strain state could exist. The criterion was determined by the width-to-depth-of-cut ratio w, which was defined as the limit of $w \geq 10$ here. Thus, y could be defined as follows:

$$y = u - 2x \tag{2}$$

$$y \geq 10h \tag{3}$$

When this criterion for y was fulfilled, this area could be calculated with a 2D simulation because a plane strain state could be expected. The remaining area (2x) was still calculated with a 3D simulation.

Using this criterion, it was possible to propose a new procedure for simulating sawing processes. As shown in Fig. 4, the approach begins with the definition of the process boundary conditions (e.g. feed per tooth) from which the depth of cut is derived. In addition, the cutting width of the cutting edge can be derived from the geometric boundary conditions. Now the defined criterion is used to decide whether a simulation should be carried out in 3D or with a division of the simulation area into 3D and 2D sections. In the case of $y < 10\,h$, the simulation should be performed in 3D, as it is expected that the edge effects in the direction of the tool cutting edge have a significant influence on the chip formation process. This means that

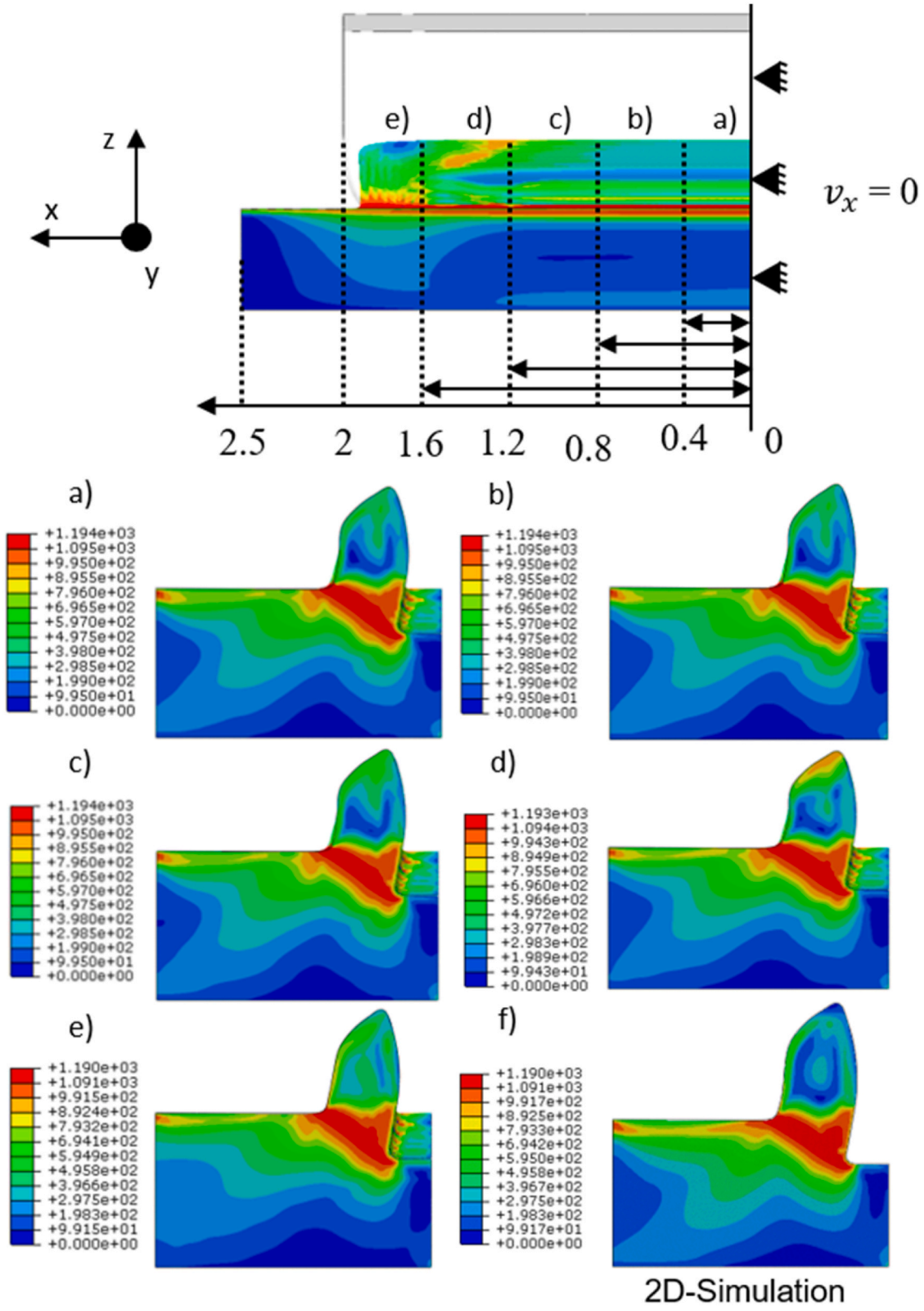

Fig. 1. Von Mises stress at different planes along the width of cut (material: AISI 1045; cutting speed 100 m/min).

the familiar procedure consisting of preprocessing, simulation and postprocessing is followed. However, if y is greater, then the simulation area can be divided according to the proposed method. This means that the secondary cutting edge and the corner radius are considered as a 3D area and the part in between as a 2D area. After the division into these areas, the usual preprocessing and simulation of the two inherent areas (3D model and 2D model) are carried out. Finally, the results of the cutting forces are combined by superposition.

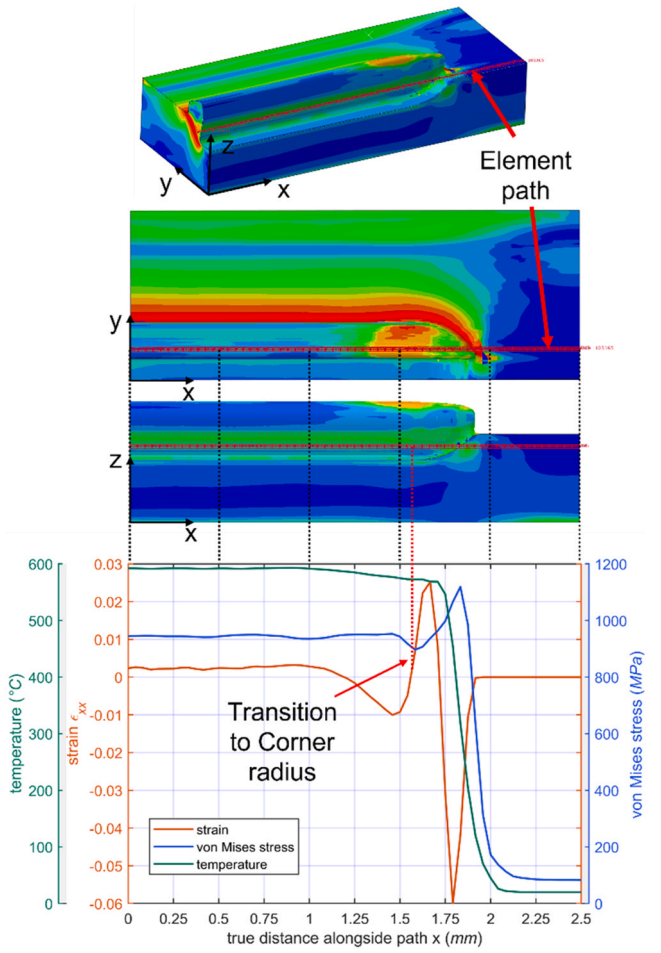

Fig. 2. Examination of von Mises stress, strain ε_{xx} (x-direction) and temperature along an element path.

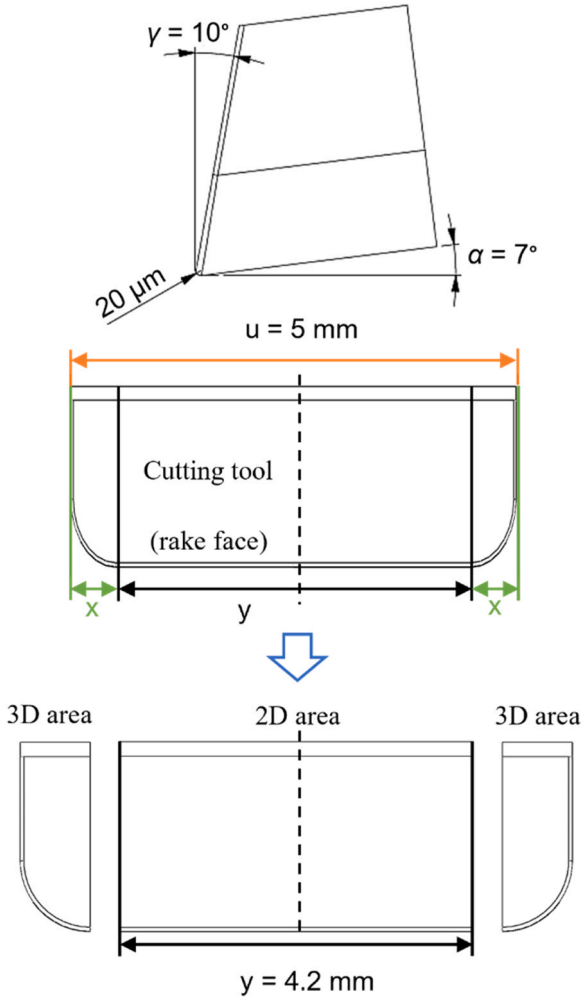

Fig. 3. Division of the cutting tool into different simulation areas.

Experimental investigation

To verify the presented method in terms of suitability, experiments were carried out which included an analysis of the cutting forces. The proposed method assumed that, for example, the cutting forces can be divided into a region of the corner radius and the secondary cutting edge (3D simulation) as well as a linear region of a plane strain state (2D simulation) by superposition of the cutting process and finally can be merged again. To investigate this procedure, special machining tests were conducted resulting in the division and analysis of the individual cutting areas, as presented in the following.

A special test rig for orthogonal cutting was used to carry out the experiments [20]. The material selected for the tests was AISI 1045 steel. As shown in Fig. 3, the tool used was an indexable insert with a rake angle of $\gamma = 10°$, a clearance angle of $\alpha = 7°$ and a cutting edge radius of 20 µm. The total tool width was 5 mm, and the corner radii were 0.4 mm. The cutting forces were measured with a Kistler 9121 three-component force measuring system. The test parameters were set as shown in Table 1.

The analysis of the cutting characteristics was carried out with a special experiment, intended to show the force properties of the individual cutting areas. In order to combine the individual results, it was essential to know the characteristics of the cutting forces in the partial areas. Furthermore, the tests were used to adjust the simulation. They were carried out three times, and the mean value was determined from the measured force traces. In addition, the chips were collected and measured. The chip thickness was determined at five positions and then averaged.

Fig. 5 shows the experimental workpiece in the test rig. The workpiece consisted of four areas. In area I, the cutting gap was designed in such a way that the entire cutting width of the tool (b = 4.2 mm) was engaged up to the transition from the corner radius to the cutting edge. This area provided information about the resulting cutting force of the corner radius and the secondary cutting edge (3D area). In area II, there was a continuous reduction down to a cutting width of b = 3 mm. From this area, it could be verified whether the cutting force increased linearly. In that case, it could be concluded that the assumption of composing a 2D and 3D simulation was physically justified, because the linear force increase showed that there are no non-linear effects due to the transition of the corner radius (3D model) to the cutting edge (2D model). Area III again showed that there is a constant force phase with a constant chip width. Finally, the entire cutting operation took place in area IV.

Fig. 6 shows the corresponding cutting forces averaged from the experiments. Area I showed an initial increase in cutting force due to the cutting engagement and was constant until the transition to area II. Area II showed a linear increase in cutting force up to area III. In area III, the cutting force was constant. In area IV, the cutting force increased again to a new constant phase.

The experiment thus proved that the assumption of a constant transition from the corner radius to the main cutting edge was valid and that the cutting force increased linearly with growing cutting width. To compare the simulation, additional free orthogonal cutting

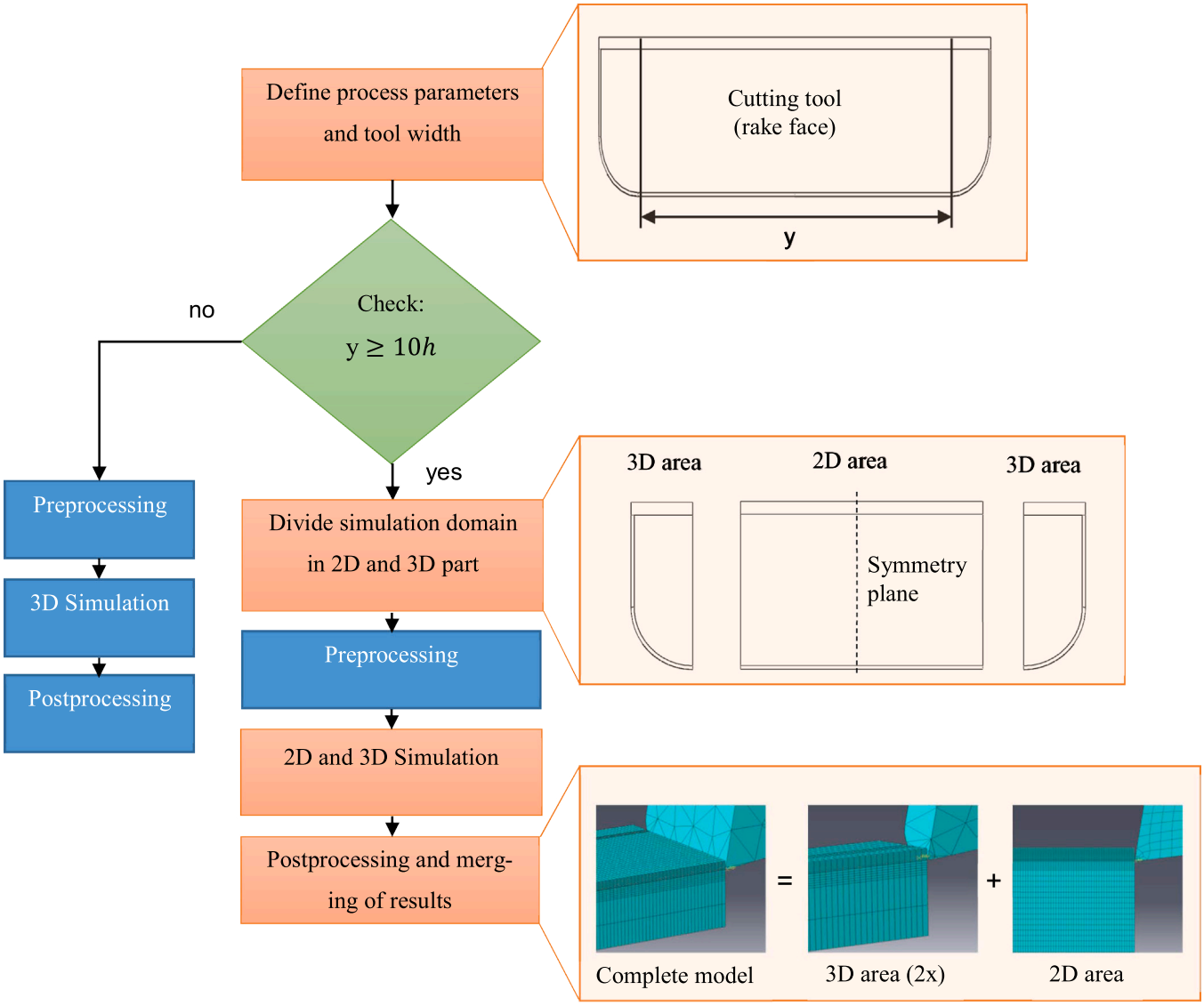

Fig. 4. New approach for simulating sawing processes.

Table 1
Test parameters.

depth of cut [mm]	0.15
cutting speed [m min^{-1}]	180
Péclet number [-]	33.5
clearance angle [°]	7
rake angle [°]	10
cutting edge radius [µm]	30

tests were carried out according to Table 1 with a cutting width of b = 3 mm. The cutting forces of the free orthogonal cut added to the cutting forces from Fig. 6b area III showed good agreement with the measured forces when the complete cutting edge was engaged (area IV). Thus, the entire bound cut could be considered as a superposition of inherent cuts in good approximation. This knowledge was used when dividing the 3D simulation into the area of the corner radius (3D simulation) and the part of the tool in between (2D simulation).

Cutting simulation

After the cutting force characteristics of the individual cutting processes were determined by experiment, the cutting process was

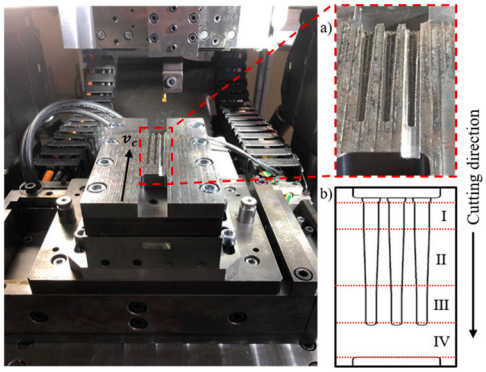

Fig. 5. Test rig for orthogonal cutting: a) detailed view of the prepared kerf; b) diagram of the cutting areas.

modelled consisting of a 3D and 2D simulation. For the cutting simulation, ABAQUS Explicit, a commercial FEM software, was used. The simulation was performed as a Lagrangian model. The chip removal was realised by element deletion in an intermediate layer. Fig. 7 shows the principal model and the boundary conditions.

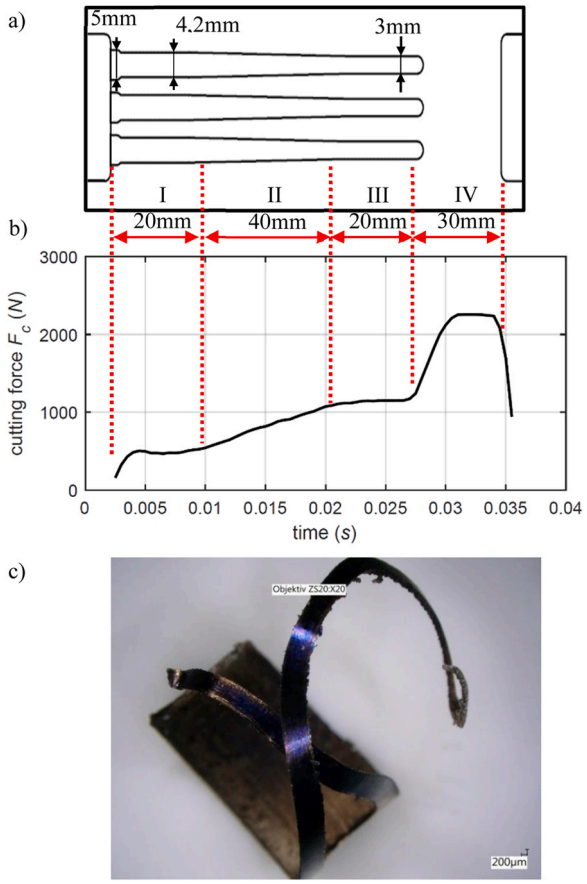

Fig. 6. Examination of the force characteristics: a) experimental workpiece; b) cutting forces at different cutting conditions, c) resulting chip.

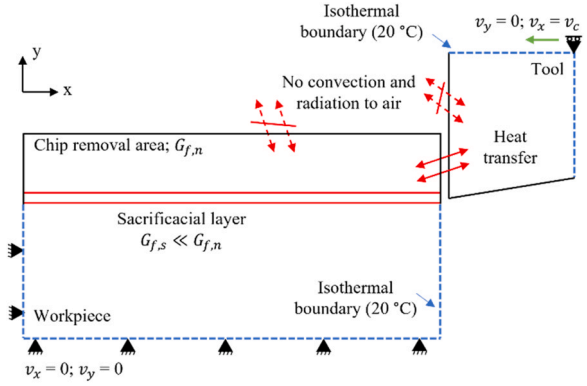

Fig. 7. Simulation model.

The widely used Johnson & Cook constitutive material model [21] was used to describe the ideal plastic yield stress of metal

$$\sigma = [A + B\varepsilon^n]\left[1 + C\ln\left(\frac{\dot{\varepsilon}}{\dot{\varepsilon}_0}\right)\right]\left[1 - \left(\frac{T - T_R}{T_m - T_R}\right)^m\right] \tag{4}$$

where A, B, n, C, and m are material-specific constants, ε is the strain, $\dot{\varepsilon}$ is the strain rate, $\dot{\varepsilon}_0$ is the reference strain rate, T is the temperature, T_m is the melting temperature and T_R is the reference temperature.

The occurrence of damage can be determined by dividing the incremental plastic strain by the fracture strain value with the following equation [22]:

$$\omega = \sum \frac{\Delta\bar{\varepsilon}}{\bar{\varepsilon}_f} \tag{5}$$

The fracture strain value is calculated here using the Johnson & Cook damage model:

$$\bar{\varepsilon}_{f,B} = [D_1 + D_2 e^{D_3\sigma^*}]\left[1 + D_4\ln\left(\frac{\dot{\varepsilon}}{\dot{\varepsilon}_0}\right)\right]\left[1 + D_5\left(\frac{T - T_R}{T_m - T_R}\right)\right] \tag{6}$$

where D1 – D5 are material-specific constants and σ^* is the stress triaxiality [23].

When $\omega = 1$, damage starts (D = 0). Then the softening regime is no longer a stress-strain relation because this would lead to a dependence of the failure on the mesh. When material softening occurs, plastic energy is dissipated. When the mesh is refined, less energy is dissipated than with a coarser mesh. To alleviate this problem, Abaqus uses the fracture energy as defined by Hillerborg [24]. Hillerborg denoted the energy G_f required to open a crack of a width w in a material as:

$$G_f = \int_{\bar{\varepsilon}_{f,B}}^{\bar{\varepsilon}_f} L\bar{\sigma}_y \mathrm{d}\varepsilon = \int_o^{\bar{u}_F} \bar{\sigma}\mathrm{d}\bar{u} \tag{7}$$

where L is the characteristic element length, $\bar{\varepsilon}_{f,B}$ is the plastic strain at the beginning of damage, $\bar{\varepsilon}_f$ is the plastic strain at failure, $\bar{\sigma}_y$ is the yield stress, $\bar{u}_F$ is the complete plastic displacement at failure. A macron denotes the plastic regime of the variable.

Dividing Eq. (7) by L converts it into a stress-strain relation. This is possible because the fracture energy in respect of the characteristic element length resembles the area under the yield stress curve at the beginning of damage, as depicted in Fig. 8. The softening of the material is defined by an exponential relation [25]:

$$D = 1 - e^{\left(-\int_0^{\bar{u}} \frac{\bar{\sigma}_y d\bar{u}}{G_f}\right)} \tag{8}$$

where D is the damage variable that denotes the loss of stiffness and the respective reduction in yield stress.

When D reaches 1 (or rather 0.99 since the exponent does not allow reaching 1 completely) the element stiffness is completely degraded. When element deletion occurs, the element is deleted and does not take part in the analysis anymore.

When there is a plane strain condition, as it can be reasonably assumed in the model for the area between the corners, G_f can be defined as [27]:

$$G_f = K_{C,I,II}^2\left(\frac{1 - \nu^2}{E}\right)(planestrain) \tag{9}$$

where $K_{C,I,II}$ is the fracture toughness for mode I (crack opening) or mode II (sliding). Within the framework of this research work, only mode I was used. The thermo-mechanical material parameters used in the simulation are depicted in Tables 2 and 3. To model the contact between the tool and the workpiece or the chip, an Aamontons/Coulomb friction coefficient of $\mu = 0.29$ was used [28,29].

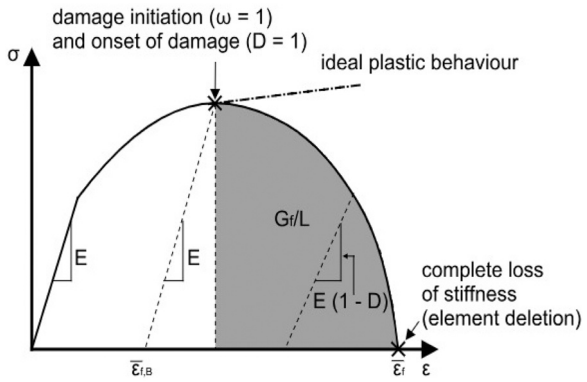

Fig. 8. Softening regime and fracture energy [25].

Table 2
Mechanical parameters and J.&C. constitutive model of AISI 1045 used in the simulation [26].

Young´s modulus [GPa]	Density [kg m^{-3}]	Poisson´s ratio [-]	A [MPa]	B [MPa]	n [-]	C [-]	m [-]	$\dot{\varepsilon}_0$ [s^{-1}]	T_m [K]	T_r [K]
200	7800	0.3	417	693	0.3266	0.745	1	0.001	1733	298.15

Although this represents a great simplification of the friction conditions, studies showed that the sticking zone decreased at higher cutting speeds [30]. Since the focus of this research was on combining the partial simulations, the simplifying assumption of a constant friction coefficient was made for the cutting conditions used here (v_c = 180 m/min and h = 0.15 mm). The following computer system was used for the simulation (Table 4):

The mesh was created with type 3D8RT elements for the 3D simulation and type CPE4RT elements (plane strain) for the 2D simulation. The simulation was carried out in several partial steps. First, the entire simulation was implemented and simulated as a pure 3D simulation (Fig. 9). To shorten the simulation time, the model was only implemented up to the middle symmetry plane. At the symmetry plane, the model had no degree of motion freedom.

In a next step, the simulation area was divided into a 2D model and a 3D model (Fig. 10), as described in Fig. 4. The 3D model contained the corner radius up to the transition to the major cutting edge. The 2D simulation contained the entire major cutting edge. The 3D simulation was carried out with 51,680 elements. The combined 2D–3D simulation consisted of 5220 elements in the 2D simulation and 18,240 elements in the 3D simulation (corner). In total, the combined 2D–3D simulation consisted of 23,460 elements.

To verify the division of the entire bound cut by combining the 3D and 2D simulations, the von Mises stress, the strain (in x-direction) and the temperature were investigated along an element path near the secondary shear zone in x-direction (compared to Fig. 2). Fig. 11 shows the results of the 2D simulation and the 3D corner simulation. It could be seen that the temperature in the 2D simulation was higher than in the 3D simulation. Moreover, the transition of the strain in the x-direction had a slight gap, even though the stresses were calculated almost identically. In sum it could be seen that the 2D simulation was generally a good approximation of the internal cutting state. Therefore, it was used to compare the resulting cutting forces, the chip thickness and the simulation time with a 3D simulation.

Results and discussion

In this section, the results of the simulation are presented and discussed. Fig. 12 shows the comparison of the cutting forces in the different simulations (3D simulation, pure 2D simulation and merged 2D–3D simulation) and in the experiment of the full cutting area (area IV). It could be seen that both the 3D simulation and the merged 2D–3D simulation led to a good agreement of the cutting forces with the values measured by experiment. Even the greatly simplified pure 2D simulation of the entire cutting width led to a good approximation to the experimental cutting force. However, the deviation was higher compared with the 3D simulation and the 2D–3D simulation.

Comparing the cutting force of the 3D simulation with the results of the merged 2D and 3D simulation showed a very good agreement. This proved that the division of the simulation area and the subsequent merging of the individual results led to a good representation of the process load properties compared with a pure 3D simulation.

Table 4
Characteristics of the workstation.

Processor	Intel (R) Core (TM) i7–7500U CPU @ 2,70 GHz
RAM	16 GB

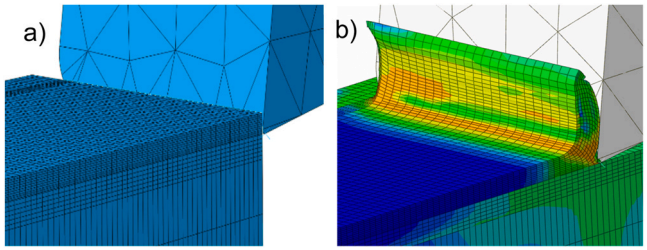

Fig. 9. 3D simulation model: a) mesh; b)formed chip.

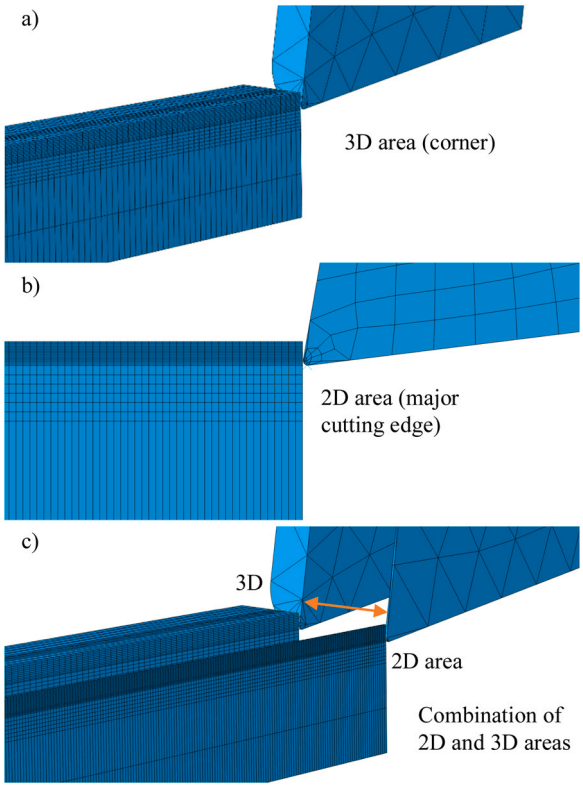

Fig. 10. Division for the inherent simulation of the sections: a) 3D simulation area b) 2D simulation area (plane strain); c) split simulation areas.

Table 3
Thermal parameters, J.&C. damage model and damage evolution parameters [26].

Thermal conductivity [W m^{-1} K^{-1}]	Specific heat capacity [J kg^{-1} K^{-1}]	Thermal expansion coefficient [K^{-1}]	Taylor-Quinney-factor [-]	D_1 [-]	D_2 [-]	D_3 [-]	D_4 [-]	D_5 [-]
50.9	486	$1.17 \cdot 10^{-5}$	0.9	0.06	3.31	-1.96	0.0018	0.58

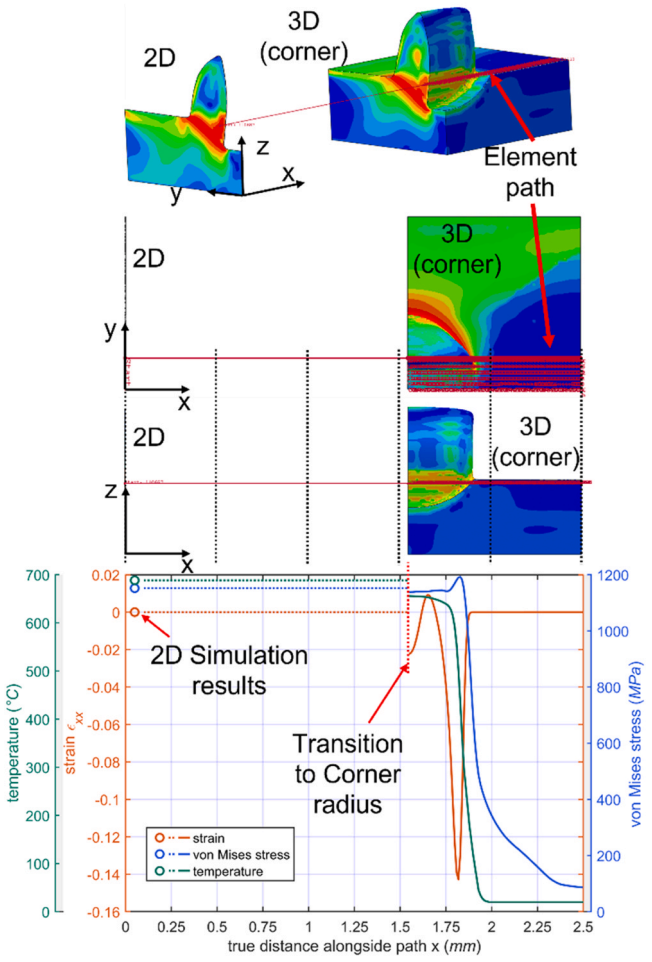

Fig. 11. Examination of von Mises stress, strain ε_{xx} (x-direction) and temperature along an element path of the merged simulation.

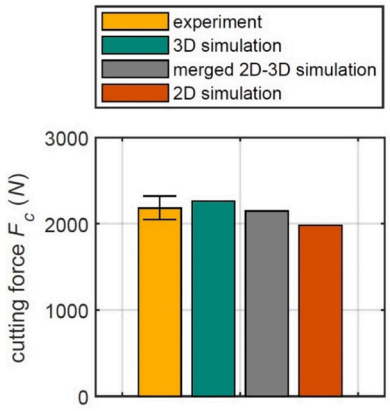

Fig. 12. Comparison of the cutting forces in the 3D simulation, the merged 2D–3D simulation, the 2D simulation and the experiments.

In addition, in Fig. 13 the simulated chip thickness of the 3D simulation was compared with the results of the partial simulations (2D model and 3D model) according to the different areas (Fig. 5). It showed that the 3D simulation (Fig. 9) agreed well with the 3D simulation when only the corner radius was engaged (Fig. 10a). Comparing the chip thickness of the 3D simulation and the 2D simulation demonstrated that the 2D simulation overestimated the chip thickness (Fig. 12).

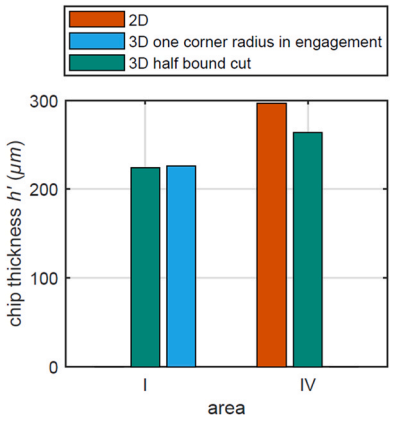

Fig. 13. Comparison of the chip thickness.

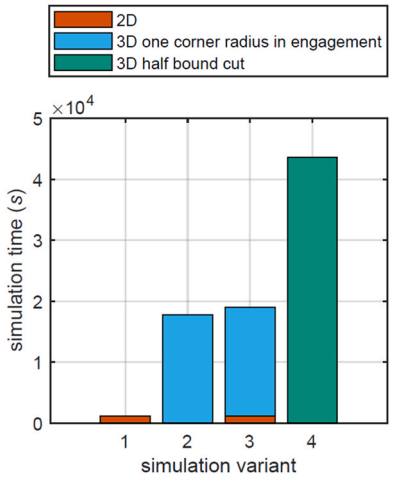

Fig. 14. Comparison of the computing time for simulation.

When comparing the simulation time of the individual models (Fig. 14), it showed that the time needed for the 2D simulation was significantly lower than for the 3D simulations. When the total simulation time of the combined 2D–3D simulation was compared with the entire 3D simulation, there was a time advantage of 56%.

Conclusions and outlook

The investigations confirmed that the proposed approach is an efficient alternative for determining the process loads occurring on a single tooth during sawing. The application was justified by the width-to-depth-of-cut ratio of w ≥ 10, since a plane strain state existed in the area between the cutting corners. The efficiency of the approach increased with growing area y. The results of the investigations can be summed up as follows:

- The required computing time is significantly shorter with the proposed approach. This is due to the lower complexity of the models and the accompanying simulation effort.
- The comparison of the process loads determined by experiment and by using a 3D simulation reveals that the cutting forces are close to reality.
- The cutting forces determined by means of a 3D simulation and the cutting forces calculated with the proposed approach are in good agreement.

In future research work, we will examine whether the results of the 2D simulation can be used as input variables for a 3D simulation.

For this purpose, the result parameters such as temperature will be calculated by a 2D simulation and then transferred to a roughly meshed 3D simulation. This would allow the simulation to be distributed across several computers. Finally, the computing time could be reduced by using a smaller number of elements. In addition, the possibility of implementing the simulation with an domain decomposition method will be investigated. This would couple the 2D area and the 3D area in a simulation and exchange field quantities between the sections. An artificial intelligence algorithm could carry out the mapping of the field sizes in the non-simulated area and thus eventually replicate an entire chip with its field sizes.

Declaration of Competing Interest

The authors declare that they have no known competing financial interests or personal relationships that could have appeared to influence the work reported in this paper.

Acknowledgements

This research was funded by the German Research Foundation (DFG) within the Priority Programme 2231 “Efficient cooling, lubrication and transportation – coupled mechanical and fluid-dynamical simulation methods for efficient production processes (FLUSIMPRO)” – project number 439925537.

References

[1] Martinez, H.V., Hankele, M., 2015. Simulation of the circular sawing process. In: Proceedings of the 10th European LS-DYNA Conference. Würzburg, Germany, pp. 15–17.
[2] Chen, Dyi-Cheng, Chen, You-Hua, You, Ci-Syong, Huang, Shin-Han, 2018, Finite element simulation and analysis of saw cutting. MATEC Web of Conferences, 185:S. 21. https://doi.org/10.1051/matecconf/201818500021.
[3] Menze, Christian, Reeber, Tim, Möhring, Hans-Christian, Stegmann, Jan, Kabelac, Stephan, 2022, Modelling of sawing processes with internal coolant supply. Manufacturing Letters, 32/2: S. 92–95. https://doi.org/10.1016/j.mfglet.2022.04.006.
[4] Arrazola, P.J., Özel, T., Umbrello, D., Davies, M., Jawahir, I.S., 2013, Recent advances in modelling of metal machining processes. CIRP Annals, 62/2: S. 695–718. https://doi.org/10.1016/j.cirp.2013.05.006.
[5] van Luttervelt, C.A., Childs, T.H.C., Jawahir, I.S., Klocke, F., Venuvinod, P.K., Altintas, Y., et al., 1998, Present situation and future trends in modelling of machining operations progress report of the CIRP Working Group ‘modelling of machining operations’. CIRP Annals, 47/2: S587–626. https://doi.org/10.1016/S0007-8506(07)63244-2.
[6] Bäker, Martin, 2006, Finite element simulation of high-speed cutting forces. Journal of Materials Processing Technology, 176/1–3: S. 117–126. https://doi.org/10.1016/j.jmatprotec.2006.02.019.
[7] Öpöz, Tahsin Tecelli, Chen, Xun, 2016, Chip formation mechanism using finite element simulation. Svazek-JME, 62/11: S. 636–646. https://doi.org/10.5545/sv-jme.2016.3523.
[8] Soliman, H.A., Shash, A.Y., El Hossainy, T.M., Abd-Rabou, M., 2020, Investigation of process parameters in orthogonal cutting using finite element approaches. Heliyon, 6/11:e05498. https://doi.org/10.1016/j.heliyon.2020.e05498.
[9] Ceretti, E., Fallböhmer, P., Wu, W.T., Altan, T., 1996, Application of 2D FEM to chip formation in orthogonal cutting. Journal of Materials Processing Technology, 59/1–2: S. 169–180. https://doi.org/10.1016/0924-0136(96)02296-0.
[10] Sridhar, Praveen, Rodríguez Prieto, Juan Manuel, Payrebrune, Kristin M. de, 2020, Discretization approaches to model orthogonal cutting with Lagrangian, Arbitrary Lagrangian Eulerian, Particle Finite Element method and Smooth Particle Hydrodynamics formulations. Procedia CIRP, 93/4: S. 1496–1501. https://doi.org/10.1016/j.procir.2020.03.139.
[11] Ducobu, F., Rivière-Lorphèvre, E., Filippi, E., 2016, Application of the Coupled Eulerian-Lagrangian (CEL) method to the modeling of orthogonal cutting. European Journal of Mechanics – A/Solids, 59:S. 58–66. https://doi.org/10.1016/j.euromechsol.2016.03.008.
[12] Menze, C., Wegert, R., Reeber, T., Erhardt, F., Moehring, H.-C., Stegmann, J., 2021, Numerical methods for the simulation of segmented chips and experimental validation in machining of TI-6AL-4V. MM SJ, 2021/5: S. 5052–5060. https://doi.org/10.17973/MMSJ.2021_11_2021152.
[13] Childs, T.H.C., 2009, Modelling orthogonal machining of carbon steels. Part I: strain hardening and yield delay effects. International Journal of Mechanical Sciences, 51/5: S. 402–411. https://doi.org/10.1016/j.ijmecsci.2009.03.007.
[14] Childs, T.H.C., Rahmad, R., 2009, Modelling orthogonal machining of carbon steels. Part II: comparisons with experiments. International Journal of Mechanical Sciences, 51/6: S. 465–472. https://doi.org/10.1016/j.ijmecsci.2009.04.001.
[15] Childs, T.H.C., 2010, Surface energy, cutting edge radius and material flow stress size effects in continuous chip formation of metals. CIRP Journal of Manufacturing Science and Technology, 3/1: S. 27–39. https://doi.org/10.1016/j.cirpj.2010.07.008.
[16] Palmer, W.B., Oxley, P.L.B., 1959, Mechanics of orthogonal machining. The Proceedings of the Institution of Mechanical Engineers, Vol 173:623–652. https://doi.org/10.1243/PIME_PROC_1959_173_053_02.
[17] Shaw, M.C., 1997, Metal Cutting Principles. Oxford University Press,.
[18] Oxley, P.L.B., 1989, The Mechanics of Machining: An Analytical Approach to assessing Machinability. Ellis Horwood,, Chichester, UK.
[19] Pednekar, Vasant, Madhavan, Vis, Adibi-Sedeh, Amir, H., 2004. Investigation of the transition from plane strain to plane stress in orthogonal metal cutting. In: Applied Mechanics. ASME 2004 International Mechanical Engineering Congress and Exposition. Anaheim, California, USA, 13.11.2004–19.11.2004: ASMEDC, S. pp. 513–528.
[20] Storchak, M., Kushner, V., Möhring, H.-C., Stehle, T., 2021, Refinement of temperature determination in cutting zones. Journal of Mechanical Science and Technology, 35/8: 36593673.
[21] G.R., Johnson, Cook, W.H., 1983. A constitutive model and data for metals subjected to large strains, high strain rates, and high temperatures. In: Proceedings of the 7th International Symposium on Ballistics. The Hague, 19–21 April 1983, pp. 541–547.
[22] Johnson, G.R., 1980. Materials characterization for computations involving severe dynamic loading. In: Proceedings of the Army Symposium on Solid Mechanics, 1980, Work in Progress. Cape Cod, Massachusetts, pp. 62–67.
[23] Johnson, Gordon R., Cook, William H., 1985, Fracture characteristics of three metals subjected to various strains, strain rates, temperatures and pressures. Engineering Fracture Mechanics, 21/1: S. 31–48. https://doi.org/10.1016/0013-7944(85)90052-9.
[24] Hillerborg, A., Modéer, M., Petersson, P.-E., 1976, Analysis of crack formation and crack growth in concrete by means of fracture mechanics and finite elements. Cement and Concrete Research, 6/6: S. 773–781. https://doi.org/10.1016/0008-8846(76)90007-7.
[25] 3DS Dassault Systems, 2021. ABAQUS 2020 Online Documentation. SIMULIA User Assistance. ⟨http://help.3ds.com/HelpProductsDS.aspx⟩.
[26] Thimm, B., 2019, Werkstoffmodellierung und Kennwertermittlung für die Simulation spanabhebender Fertigungsprozesse (Dissertation). Institut für Werkstofftechnik, Universität Siegen, Siegen.
[27] Mabrouki, Tarek, Girardin, François, Asad, Muhammad, Rigal, Jean-François, 2008, Numerical and experimental study of dry cutting for an aeronautic aluminium alloy (A2024-T351. International Journal of Machine Tools and Manufacture, 48/11: S. 1187–1197. https://doi.org/10.1016/j.ijmachtools.2008.03.013.
[28] Ben Abdelali, H., Claudin, C., Rech, J., Ben Salem, W., Kapsa, Ph, Dogui, A., 2012, Experimental characterization of friction coefficient at the tool–chip–workpiece interface during dry cutting of AISI 1045. Wear, 286–287/J10: S. 108–115. https://doi.org/10.1016/j.wear.2011.05.030.
[29] Afrasiabi, Mohamadreza, Saelzer, Jannis, Berger, Sebastian, Iovkov, Ivan, Klippel, Hagen, Röthlin, Matthias, et al., 2021, A numerical-experimental study on orthogonal cutting of AISI 1045 Steel and Ti6Al4V alloy: SPH and FEM modeling with newly identified friction coefficients. Metals, 11/11: S. 1683. https://doi.org/10.3390/met11111683.
[30] Abouridouane, Mustapha, Bergs, Thomas, Schraknepper, Daniel, Wirtz, Guido, 2021, Friction behavior in metal cutting: modeling and simulation. Procedia CIRP, 102:S. 405–410. https://doi.org/10.1016/j.procir.2021.09.069.